J Mater Sci: Mater Electron (2018) 29:1542–1553
DOI 10.1007/s10854-017-8064-2

# Barium ferrite prepared by modified Pechini method: effects of chloride and nitrate counter ions on microstructures and magnetic properties

**Worawat Wattanathana[1] · Worawut Nantharak[1] · Suttipong Wannapaiboon[2] · Pongsakorn Jantaratana[3] · Chatchai Veranitisagul[4] · Nattamon Koonsaeng[5] · Apirat Laobuthee[1]**

Received: 25 July 2017 / Accepted: 14 October 2017 / Published online: 2 November 2017


**Abstract** Barium hexaferrite powders were successfully prepared by the modified Pechini method using citrate and glycerol. The materials were prepared employing different Ba:Fe ratios, iron(III) precursors and calcination temperatures. The obtained powders were characterized by XRD, VSM, SEM, EDX and FT-IR. The Ba:Fe molar ratio of 1:11, for both chloride and nitrate series, is observed to be the optimal ratio to attain the phase-pure barium hexaferrite. Moreover, these barium hexaferrite powders synthesized with the Ba:Fe ratio of 1:11 showed the highest saturation magnetization among the samples in the same series. Interestingly, the powders formed from chloride precursors had significantly lower coercive fields than those from nitrate precursors, highlighting the role of counter ions. The reasons were likely to be the smaller particle sizes in materials obtained from the nitrate precursors and possibly the distortion of the barium hexaferrite structure due to the substitution of some oxide with the chloride species within the materials obtained in the chloride series.

✉ Apirat Laobuthee
fengapl@ku.ac.th

[1] Department of Materials Engineering, Faculty of Engineering, Kasetsart University, Chatuchak, Bangkok 10900, Thailand

[2] Synchrotron Light Research Institute (Public Organization), 111 University Avenue, Suranaree, Muang, Nakhon Ratchasima 30000, Thailand

[3] Department of Physics, Faculty of Science, Kasetsart University, Chatuchak, Bangkok 10900, Thailand

[4] Department of Materials and Metallurgical Engineering, Faculty of Engineering, Rajamangala University of Technology Thanyaburi, Klong 6, Thanyaburi 12110, Pathumthani, Thailand

[5] Department of Chemistry, Faculty of Science, Kasetsart University, Chatuchak, Bangkok 10900, Thailand

## 1 Introduction

Ferrites are one type of ceramic materials that have received significant attention in scientific community during the last decades due to their promising magnetic properties. Interestingly, magnetic properties of ferrites can be controlled by alteration of the crystal structures and tuning of the chemical (atomic) compositions, resulting in a variety of coercivity and remanence of the different ferrites after magnetization and consequently a broad range of applicability [1–8]. On one hand, soft ferrites e.g. zinc ferrite, which exhibit a low coercivity and can be easily altered their magnetization direction without dissipating much energy, could be a good candidate for applying in transformers and electromagnetic cores. On the other hand, hard magnetic ferrites such as barium hexaferrite, $BaFe_{12}O_{19}$, with spinel structure have been widely investigated due to its large magneto crystalline anisotropy, high Curie temperature, high saturation magnetization ($M_s$), high coercive field ($H_c$) and excellent chemical stability as well as corrosion resistivity [9–14]. Due to its promising properties, barium hexaferrite has been used in various applications such as permanent magnets in storage media, electrical power generation and distribution [10], disk drivers and video recorders [14]. In order to get the properties required for the mentioned applications, such as ultrafine powder for use in high density magnetic recording media, synthetic conditions and methods need to be studied and optimized.

For many years, there has been much research reporting synthetic routes for barium hexaferrite materials such as solid-state reactions between the constitute oxides and/or

carbonates [15, 16]. The main disadvantages of this method are the occurrence of impure phases and inhomogeneity of the products. To get the pure phase of barium hexaferrite by this method, high temperature and long calcination time are usually applied. In order to solve this problem, chemical syntheses such as hydrothermal method [17, 18], microemulsion process [19], glass crystallization [20], chemical co-precipitation [21–23], sol–gel method [24–26], colloidal synthesis [27], organic resin method [28] and aerosol synthesis method [29] have been alternatively used. The Pechini method appears to have attracted much attention in the recent years due to the achievement in synthesis of homogeneous and ultrafine barium hexaferrite at a relatively low calcination temperature [30].

Although barium hexaferrite has been studied in many works, the optimum molar ratio of Ba:Fe to achieve pure phase has not been clearly reported. Meng et al. [30] successfully synthesized barium hexaferrite single phase via sol–gel combustion technique with Ba:Fe molar ratio of 1:9. Carp et al. [31] presented that the pure barium hexaferrite phase was obtained at Ba:Fe molar ratio of 1:10.5. Mendoza-Suarez et al. [32] and Yen-Pei et al. [33] reported that Ba:Fe molar ratio to get the barium hexaferrite single phase should be around 1:11 when the obtained powders were prepared from sol–gel and microwave induced combustion methods, respectively. The low temperature combustion method was applied by Huang et al. [34] to produce the pure phase of barium hexaferrite with Ba:Fe molar ratio of 1:11.5. Mendoza-Suarez et al. [35] prepared pure barium hexaferrite with Ba:Fe molar ratio of 1:12 by using the ball milling technique. Note that, the optimum Ba:Fe ratio reported in the literatures was varied, which could be assigned to the different synthetic methods employed. Apart from the synthetic methods, the metal sources were considered to be the other influent factor. To clarify this point, we herein studied the effects of starting materials, Ba:Fe molar ratios, and calcination temperature on phase composition, microstructures, and magnetic properties of the barium hexaferrite synthesized by the modified Pechini method.

## 2 Experimental

### 2.1 Materials synthesis

The starting materials, barium nitrate ($Ba(NO_3)_2$) and difference iron salts ($FeCl_3$ and $Fe(NO_3)_3{\cdot}9H_2O$) were firstly dissolved in 10 ml distilled water to form a clear aqueous solution. The Ba:Fe molar ratio was varied from 1:9 to 1:12. 10 ml of glycerol was further added into the solution to chelate $Ba^{2+}$ and $Fe^{3+}$ and form the complex precursors. The mixture solutions were heated to 120 °C on a hot plate with magnetic stirring. After water was evaporated, the solution became viscous and finally formed very viscous brown dried gels. Then, the dried gels were transferred to an autoclave and heated in an oven with the temperature of 80 °C for 24 h to get the barium hexaferrite precursors. Further, the precursors were calcined in the ambient atmosphere at different temperatures (800–1200 °C) to obtain the powder products.

### 2.2 Materials characterization

Fourier-Transform infrared (FTIR) spectra were recorded by a Fourier-Transform infrared spectrophotometer (Bruker, Alpha FT-IR spectrometer). The sample powders were finely ground with KBr and pressed into pellets before measurement. All the peaks in the range 4000–375 $cm^{-1}$ were recorded with spectral resolution of 2 $cm^{-1}$.

The phase compositions of the obtained powders were determined by X-ray diffraction (XRD, X'PertPRO MPD diffractometer) using Cu Kα radiation. Diffraction patterns were recorded over the range of 2θ angles from 10° to 90° in step-scanning mode (0.02° steps with a step counting time of 2 s).

The morphology of the samples was observed by a Scanning Electron Microscope (SEM, XL30 series, Phillips) operating at an acceleration voltage of 13–15 kV and magnification value of ×5000. Samples were mounted on stubs using carbon tape and then sputtered with Au prior to the SEM measurements.

All the resulting powders were pressed into pellets with the same pressure of 10 MPa. The magnetic properties in terms of saturation magnetization ($M_s$), magnetic remanence or remanent magnetization ($M_r$) and coercivity ($H_c$) were measured by a vibrating sample magnetometer (VSM) with a maximum applied field of 10,000 Oe by using nickel as a standard.

## 3 Results and discussion

### 3.1 Effect of Ba:Fe molar ratio on the phase compositions and magnetic properties

The powders obtained after the calcination at a temperature of 1200 °C for 2 h in the ambient atmosphere were studied in the phase compositions by using an X-ray diffractometer. Figure 1 shows the XRD patterns of the powders synthesized from barium nitrate and iron(III) chloride as metal sources with various Ba:Fe molar ratios of 1:9, 1:10, 1:11 and 1:12, respectively. The results show that the single barium hexaferrite ($BaFe_{12}O_{19}$) (JCPDS. No. 74-1121) phase can be obtained from the Ba:Fe molar ratio of 1:11. There was a minor barium monoferrite ($BaFe_2O_4$) (JCPDS. No. 25-1191) phase coexisting with barium hexaferrite when the Ba:Fe molar ratios were 1:9 and 1:10. The occurrence of barium monoferrite can be explained as there were not

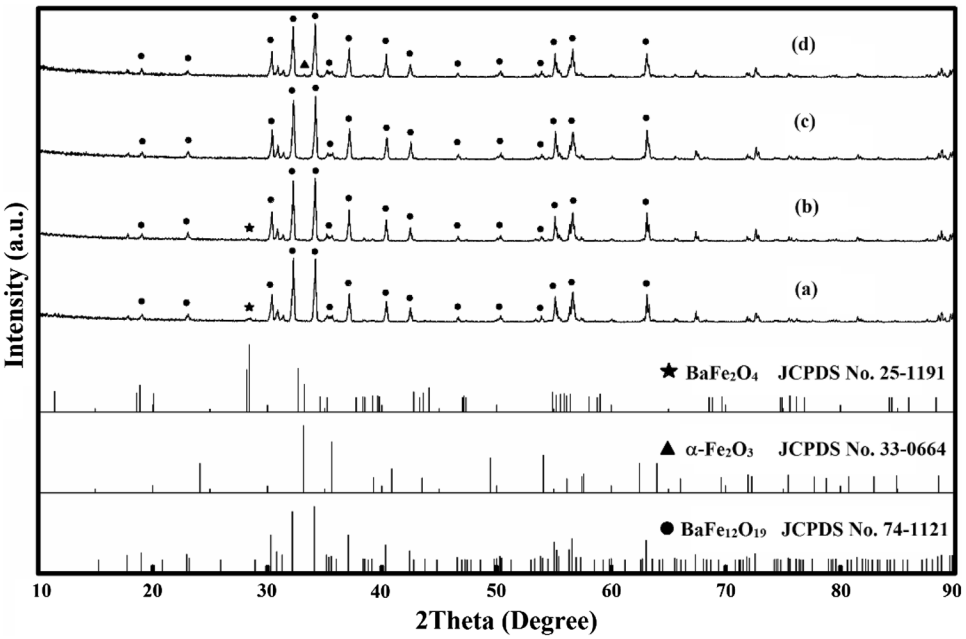


**Fig. 1** XRD patterns for the obtained powders after calcined at 1200 °C of the metal complex precursors prepared from barium nitrate and iron(III) chloride (the chloride series) with various Ba:Fe molar ratio *a* 1:9, *b* 1:10, *c* 1:11 and *d* 1:12

enough iron ions (in other words, barium ions were excessive) to completely form phase-pure barium hexaferrite. Hence, the barium monoferrite, which was required lower content of iron ions than in the formation of barium hexaferrite, was attempted to form as the minor phase when using the deficient amount of iron source in the synthesis (e.g. 1:9 and 1:10 Ba:Fe ratio). On the other hand, the Ba:Fe molar ratio of 1:12 yielded the barium hexaferrite phase with a little amount of α-hematite phase (α-$Fe_2O_3$) (JCPDS. No. 33-0664). This meant that there were too many iron ions for the formation of single-phase barium hexaferrite or not enough barium ions to entirely form the barium hexaferrite phase. Therefore, the excess iron ions were forced to form their oxide phase instead. According to the XRD results of barium hexaferrites synthesized from iron chloride, the most suitable Ba:Fe molar ratio in order to get the phase-pure barium hexaferrite was 1:11.

Furthermore, the barium hexaferrite powders were synthesized by calcining the complex precursors formed by using barium nitrate and iron(III) nitrate as metal sources with the various Ba:Fe molar ratios at 1200 °C for 2 h in the air (XRD patterns of the obtained products were illustrated in Fig. 2). Note that, the Ba:Fe molar ratio of 1:11 was also found to be the proper molar ratio of the metal sources in order to achieve the phase-pure barium hexaferrite phase. Again, the XRD pattern of the powder product with Ba:Fe molar ratio of 1:12 showed a little amount of α-hematite phase mixed with the barium hexaferrite phase as also observed from chloride salt. Barium monoferrite was also observed in the XRD patterns of the calcined products from nitrate salts with the Ba:Fe molar ratios of 1:9 and 1:10. This result was similar to the one observed in cases of using the iron(III) chloride salt but the relative intensity of the barium monoferrite peak in the XRD patterns herein was higher. Moreover, the α-hematite was also found as the minor phase. Since the iron ions were not excessive in this case, the reason for the presence of α-hematite was the incompletion of the reaction between barium monoferrite and α-hematite to get the desired product, barium hexaferrite. However, the further increase of the amount of iron ions can reduce the amounts of barium monoferrite phase as the reaction of barium monoferrite with iron to form barium hexaferrite phase was endorsed.

Lattice constants, a, b and c, of the prepared powders were refined from the Eq. 1, where h, k and l are miller indexes, and d is interplanar distance. Here, the planes (107) and (114) of barium hexaferrite phase were used for the calculation. Then, lattice parameters, a, b and c, obtained from Eq. 1 were used to determine lattice volume (V) according to Eq. 2. X-ray density ($\rho_x$) can be determined by using Eq. 3, where M is the molecular weight of the barium hexaferrite, N is Avogadro's number and 2 stands for the number of formula units in a cell.

$$\frac{1}{d^2} = \frac{4}{3}\left(\frac{h^2 + k^2 + hka}{2}\right) + \frac{l^2}{c^2} \tag{1}$$

$$V = \sqrt{1 + 2\cos(\alpha)\cos(\beta)\cos(\gamma) - \cos^2(\alpha) - \cos^2(\beta) - \cos^2(\gamma)} \tag{2}$$

$$\rho_x = \frac{2M}{NV} \tag{3}$$

As shown in the Tables 1 and 2, the intermediate phases, α-hematite and barium monoferrite, presented in the

obtained powders affected the length of the c axis and the lattice volume and X-ray density. From the nitrate series, the lattice parameters, lattice volume and X-ray density of the calcined powder are similar to the standard barium hexaferrite (JCPDS No. 74-1121). Note that, the product obtained from the synthesis using the Ba:Fe molar ratio of 1:11 shows the closest values to the standard one. This was in agreement with the XRD and VSM results. However, the mentioned values for the calcined powders obtained in the chloride series were deviated, of which no calcined powders had similar parameters to the standard one. Apart from the impure phases, it would be other factors to alter the lattice

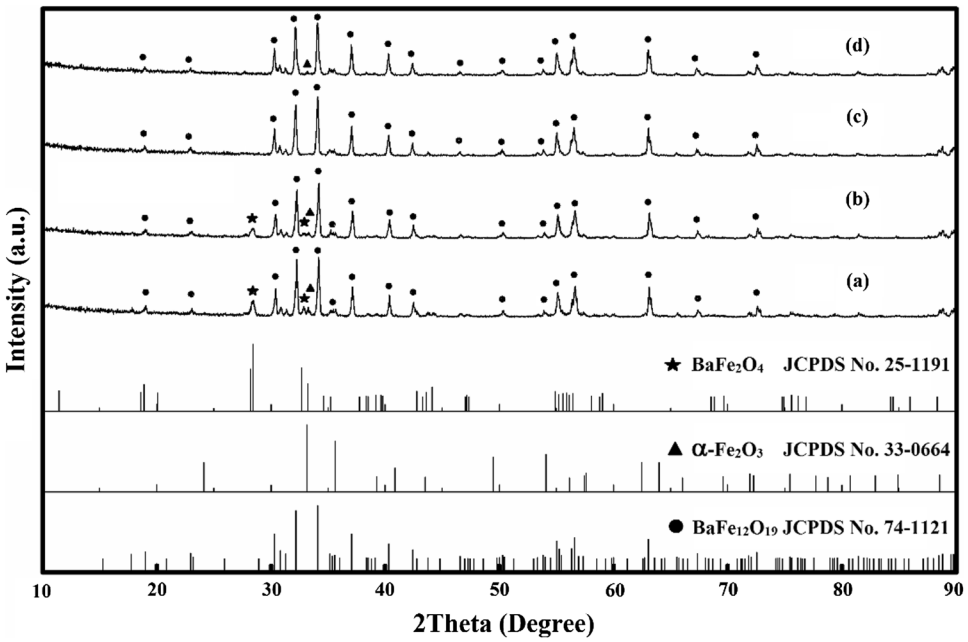


**Fig. 2** XRD patterns for the obtained powders after calcined at 1200 °C of the metal complex precursors prepared from barium nitrate and iron(III) nitrate (the nitrate series) with various Ba:Fe molar ratio *a* 1:9, *b* 1:10, *c* 1:11 and *d* 1:12

**Table 1** Lattice constants (a, b and c), lattice volume (V), X-ray density ($\rho_x$), saturation magnetization ($M_s$), remanent magnetization ($M_r$) and coercivity ($H_c$) of the obtained powders after calcined at 1200 °C using the metal complexes formed by barium nitrate and iron(III) chloride salts with various Ba:Fe molar ratios

| Parameters | JCPDS No. 74-1121 | Ba:Fe = 1:9 | Ba:Fe = 1:10 | Ba:Fe = 1:11 | Ba:Fe = 1:12 |
|---|---|---|---|---|---|
| a (Å) | 5.8930 | 5.8780 | 5.8881 | 5.8712 | 5.8790 |
| b (Å) | 5.8930 | 5.8780 | 5.8881 | 5.8712 | 5.8790 |
| c (Å) | 23.1940 | 23.1799 | 23.1714 | 23.1679 | 23.1513 |
| V (Å$^3$) | 697.5600 | 693.5951 | 695.7239 | 691.6257 | 692.9540 |
| $\rho_x$ (g/cm$^3$) | 5.2900 | 5.3212 | 5.3049 | 5.3364 | 5.3261 |
| $M_s$ (emu/g) | | 48.7081 | 53.0033 | 53.0850 | 49.6452 |
| $M_r$ (emu/g) | | 18.0351 | 18.6583 | 16.6540 | 15.5592 |
| $M_r/M_s$ | | 0.3703 | 0.3520 | 0.3137 | 0.3134 |
| $H_c$ (kOe) | | 0.6180 | 0.6410 | 0.5040 | 0.5820 |

**Table 2** Lattice constants (a, b and c), lattice volume (V), X-ray density ($\rho_x$), saturation magnetization ($M_s$), remanent magnetization ($M_r$) and coercivity ($H_c$) of the obtained powders after calcined at 1200 °C using the metal complexes formed by barium nitrate and iron (III) nitrate salts with various Ba:Fe molar ratios

| Parameters | JCPDS No. 74-1121 | Ba:Fe = 1:9 | Ba:Fe = 1:10 | Ba:Fe = 1:11 | Ba:Fe = 1:12 |
|---|---|---|---|---|---|
| a (Å) | 5.8930 | 5.8809 | 5.8876 | 5.8952 | 5.8897 |
| b (Å) | 5.8930 | 5.8809 | 5.8876 | 5.8952 | 5.8897 |
| c (Å) | 23.1940 | 23.1455 | 23.1356 | 23.2241 | 23.1388 |
| V (Å$^3$) | 697.5600 | 693.2493 | 694.5315 | 698.974 | 695.1168 |
| $\rho_x$ (g/cm$^3$) | 5.2900 | 5.3239 | 5.3140 | 5.2802 | 5.2690 |
| $M_s$ (emu/g) | | 47.3251 | 45.1666 | 54.0514 | 50.1282 |
| $M_r$ (emu/g) | | 26.0525 | 26.3764 | 31.6237 | 29.4242 |
| $M_r/M_s$ | | 0.5505 | 0.5840 | 0.5851 | 0.5870 |
| $H_c$ (kOe) | | 1.5140 | 2.2640 | 2.1539 | 2.4890 |

parameters, lattice volume and X-ray density, for example the substitution of remaining chloride to the lattice at the position of oxygen atoms. This would be the reason why the coercive fields of all the materials prepared from the chloride series were comparatively low compared to the nitrate series, in which the nitrate ions were much easier to eliminate from the barium hexaferrite lattice.

The magnetic properties of the obtained powders with various Ba:Fe molar ratios of 1:9, 1:10, 1:11 and 1:12 were investigated by vibrating sample magnetometer (VSM). Hysteresis loops of the calcined powders obtained from the iron(III) chloride precursor with the different Ba:Fe ratios (1:9, 1:10, 1:11 and 1:12) are illustrated in Fig. 3. It was observed that the powders with the Ba:Fe ratios of 1:10 and 1:11 showed the highest saturation magnetization. The saturation magnetization ($M_s$) values for the powders with 1:10 and 1:11 were 53.0033 and 53.0850 emu/g, respectively. However, the calcined powder with the Ba:Fe ratio of 1:10 gave the greatest magnetic remanence ($M_r$) of 18.6583 emu/g. These results supported the results from XRD that the powder prepared using the Ba:Fe ratio of 1:11 gave the pure phase of hard magnetic barium hexaferrite. The obtained powder with the Ba:Fe ratio of 1:9 had lower $M_s$ and $M_r$ values due to the presence of the antiferromagnetic $BaFe_2O_4$ [30]. The $M_s$ and $M_r$ values of the powder with the Ba:Fe ratio of 1:12 was the lowest due to α-hematite impurity [30]. However, the trend of coercivity did not show such a clear-cut. As seen from Table 1, the coercivity ($H_c$) of the prepared powder using the Ba:Fe ratio of 1:11 was the lowest even though it was the pure phase of barium hexaferrite. Hence, there would be the other factors that affect the coercive field. Hysteresis loops for all the samples prepared from the nitrate series are depicted in Fig. 4. Again the Ba:Fe ratio of 1:11 yielded the pure barium hexaferrite with the highest $M_s$ and $M_r$ values. The other powders with impurities had lower saturation and remanence magnetizations. Here it was easy to notice that the powder with the Ba:Fe ratio of 1:9 had a comparatively lower coercive field than those other samples as it contained the largest amount of antiferromagnetic $BaFe_2O_4$. When compared with the powders prepared from the nitrate series with the chloride ones, all the powders prepared from the nitrate series possessed slightly higher saturation magnetization but significantly higher coercivity. This result led to the conclusion that the saturation magnetization of magnetic materials depended mainly on the phase composition while the coercivity leaned on the phase composition as well as the other factors such as counter ions.

### 3.2 Effect of calcination temperature on the phase composition, microstructure and magnetic properties

In this part, the metal complex precursors obtained from both the iron(III) chloride and iron(III) nitrate salts were prepared with the fixed Ba:Fe molar ratio of 1:11 in order to synthesize barium hexaferrite materials. The obtained metal complex precursors were calcined at different temperatures (i.e. 800, 900 1000, 1100 and 1200 °C) for 2 h in ambient atmosphere. Phase compositions, microstructures and magnetic properties were determined by XRD, SEM and VSM, respectively. Figure 5 shows the XRD patterns of the calcined powders derived from the chloride series. The results indicated that the obtained powders after being calcined at 800–1000 °C had the α-hematite as a major phase. Moreover,

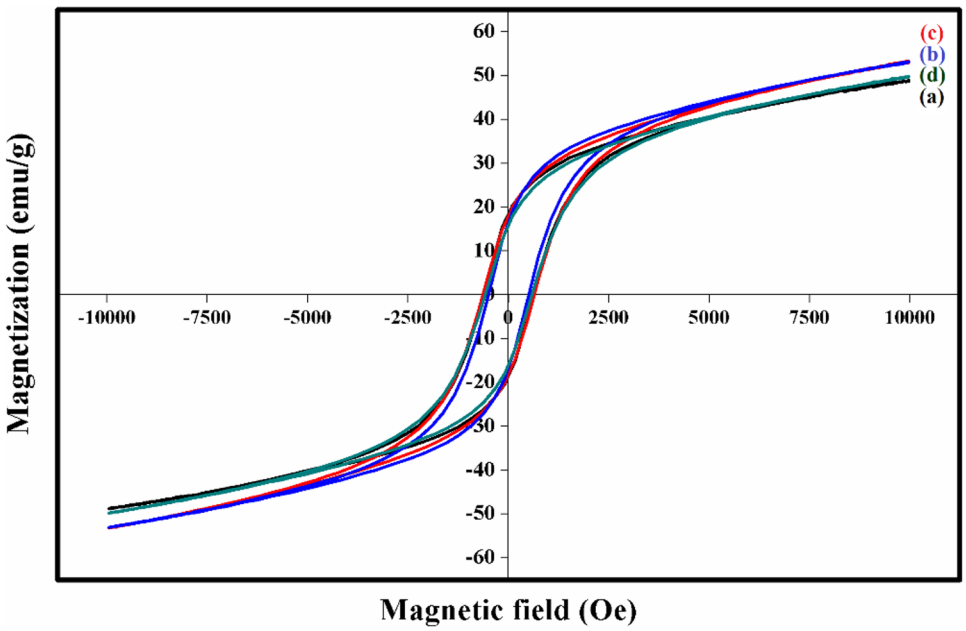


**Fig. 3** VSM hysteresis loops for the obtained powders after calcined at 1200 °C of the metal complex precursors prepared from barium nitrate and iron(III) chloride (the chloride series) with various Ba:Fe molar ratios *a* 1:9, *b* 1:10, *c* 1:11 and *d* 1:12

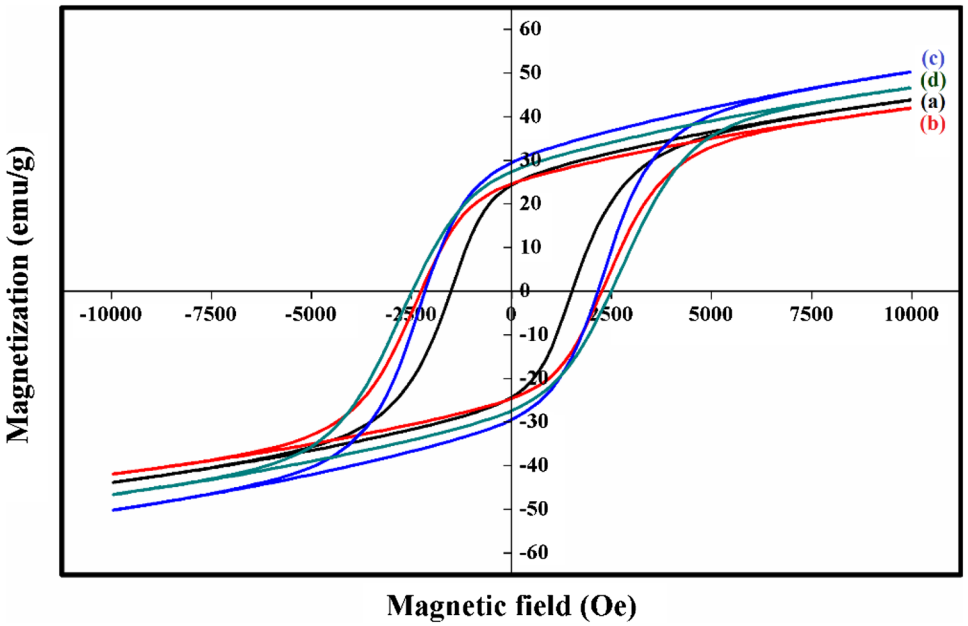


**Fig. 4** VSM hysteresis loops for the obtained powders after calcined at 1200 °C of the metal complex precursors prepared from barium nitrate and iron(III) nitrate (the nitrate series) with various Ba:Fe molar ratios *a* 1:9, *b* 1:10, *c* 1:11 and *d* 1:12

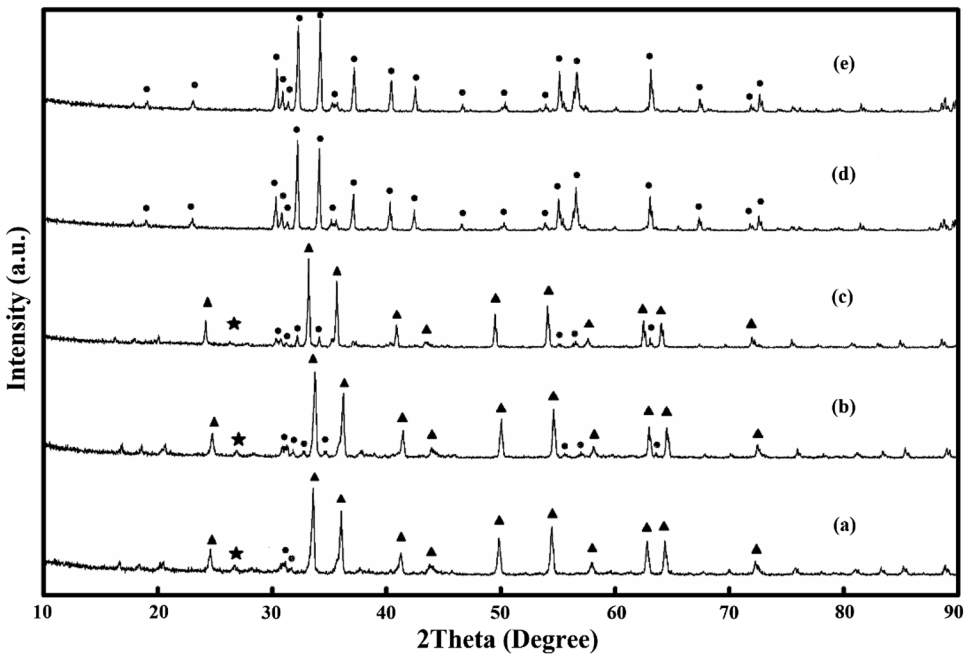


**Fig. 5** XRD patterns for the obtained powders after calcining the metal complex precursors of the chloride series with Ba:Fe molar ratio of 1:11 at different temperatures *a* 800, *b* 900, *c* 1000, *d* 1100 and *e* 1200 °C; Note that, the phase formations are indexed in the similar fashion with illustrated in Figs. 1 and 2

the barium monoferrite phase was also detected. Even if the calcination temperature was up to 1000 °C, the barium hexaferrite peaks were still weak (observed as a minor phase). However, if the calcination temperature was up to 1100 °C, the barium monoferrite and α-hematite phase were totally wiped out resulting in the pure barium hexaferrite phase. The calcination temperature of 1200 °C also yielded the pure barium ferrite phase with higher intensity and crystallinity. Hence, the phase transformation of the chloride complex precursors to form as the barium hexaferrite with spinel structure can be shown as the equations below.

$$\text{Precursor} \rightarrow \alpha\text{-}Fe_2O_3\ (\text{major phase}) + BaFe_2O_4 + BaFe_{12}O_{19} \ldots (800 - 1000\,^{o}\text{C})$$

$$\alpha\text{-}Fe_2O_3 + BaFe_2O_4 + BaFe_{12}O_{19} \rightarrow BaFe_{12}O_{19} \ldots (1100 - 1200\,^{o}\text{C})$$

The powders obtained after calcining the metal complex precursor of the nitrate series at temperatures (800, 900

1000, 1100 and 1200 °C) for 2 h were studied by the same means as in case of the chloride series. According to XRD results in Fig. 6, the mixed phase of barium hexaferrite, α-hematite and barium monoferrite phases were detected when calcining the precursors at temperature of 800 °C. The intensities of the barium hexaferrite peaks were crucially higher than the peaks at 800 °C of the powder obtained from the chloride series. Specifically, the barium hexaferrite peaks were found only at temperatures of 1100 °C and higher in the chloride series, while they were started to be found at 800 °C in the nitrate series. Therefore, chloride ion was likely to be the inhibitor for the formation of barium hexaferrite phase. If the calcination temperature was increased from 800 to 900 °C, nearly complete barium hex aferrite phase was obtained and the intermediate phases (α-hematite and barium monoferrite) were explicitly decreased. The crystalline phase-pure barium hexaferrite was found at the minimum calcination temperature of 1000 °C. The calcination temperatures of 1100 and 1200 °C would also give phase-pure barium hexaferrite phase with higher intensity XRD peaks and also crystallinity. Hence, the phase transformation of the metal complex precursor of the nitrate series to form the barium hexaferrite can be shown by the equations below.

$$\text{Precursor} \rightarrow \alpha\text{-}Fe_2O_3 + BaFe_2O_4 + BaFe_{12}O_{19}\,(\text{major phase}) \ldots (800\,^{\circ}\text{C} - 900\,^{\circ}\text{C})$$

$$\alpha\text{-}Fe_2O_3 + BaFe_2O_4 + BaFe_{12}O_{19} \rightarrow BaFe_{12}O_{19} \ldots (1000 - 1200\,^{\circ}\text{C})$$

The magnetic properties of the obtained powders with the fixed Ba:Fe molar ratio at 1:11 but varied the calcination temperatures (800–1200 °C) using iron(III) chloride and iron(III) nitrate are shown in Figs. 7 and 8 and Tables 3 and 4. The trend of saturation magnetization was in line with the XRD results. For the chloride series, the hard-magnetic barium hexaferrite began to form at 1100 °C so that the saturation magnetization was increased sharply when the calcination temperature was changed from 1000 to 1100 °C. For the nitrate series, the barium hexaferrite was observed in all the calcination temperatures employed in the study so that there was no sharp change in the magnetic property observed in the obtained powders in the nitrate series. The saturation magnetization gradually increased as the calcination temperature was increased from 800 to 1100 °C. The maximum saturation magnetization was at 1100 °C, as this was the lowest temperature that provided the pure barium ferrite phase. The result confirmed that the saturation magnetization depended mainly on the phase composition. The calcination of 1200 °C gave rise to the decrease in the saturation magnetization and coercivity. This would be the result of the agglomeration of the particles and the change in the size of the magnetic domain of barium hexaferrite product when the particles were agglomerated. Like the results observed in the first part of this work, the coercivity of the materials from the nitrate series was essentially larger than those of the powders obtained from the chloride series. The factor that had an influence on the great difference in coercivity was not the phases, as the XRD results showed that at calcination temperatures of 1100 °C and above, in both the chloride and nitrate precursors offered the pure barium hexaferrite phases. Therefore, further investigation would be needed.

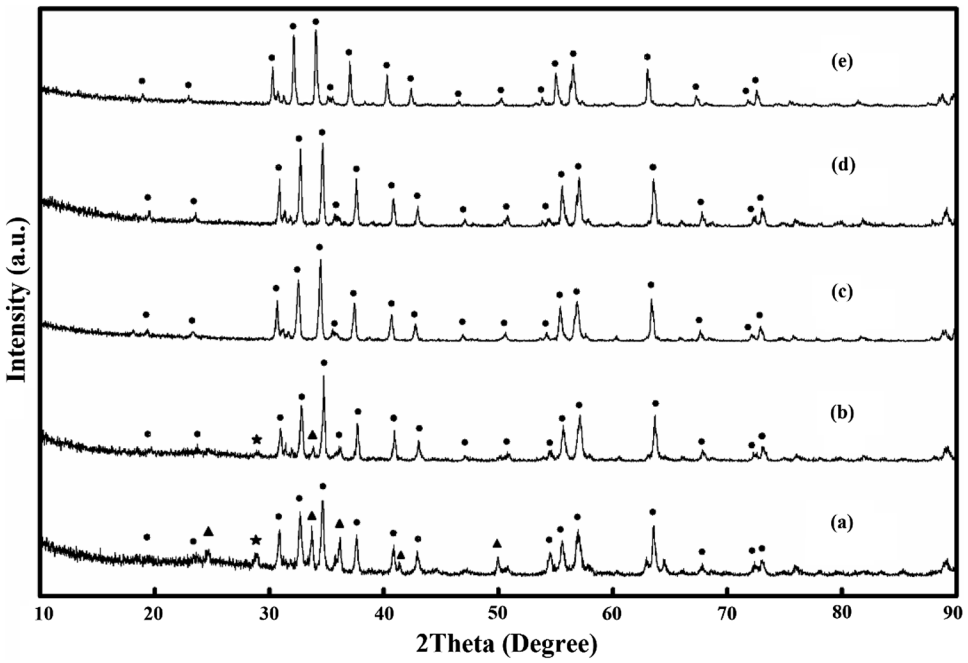


**Fig. 6** XRD patterns for the obtained powders after calcining the metal complex precursors of the nitrate series with Ba:Fe molar ratio of 1:11 at different temperatures *a* 800, *b* 900, *c* 1000, *d* 1100 and *e* 1200 °C; Note that, the phase formations are indexed in the similar fashion with illustrated in Figs. 1 and 2

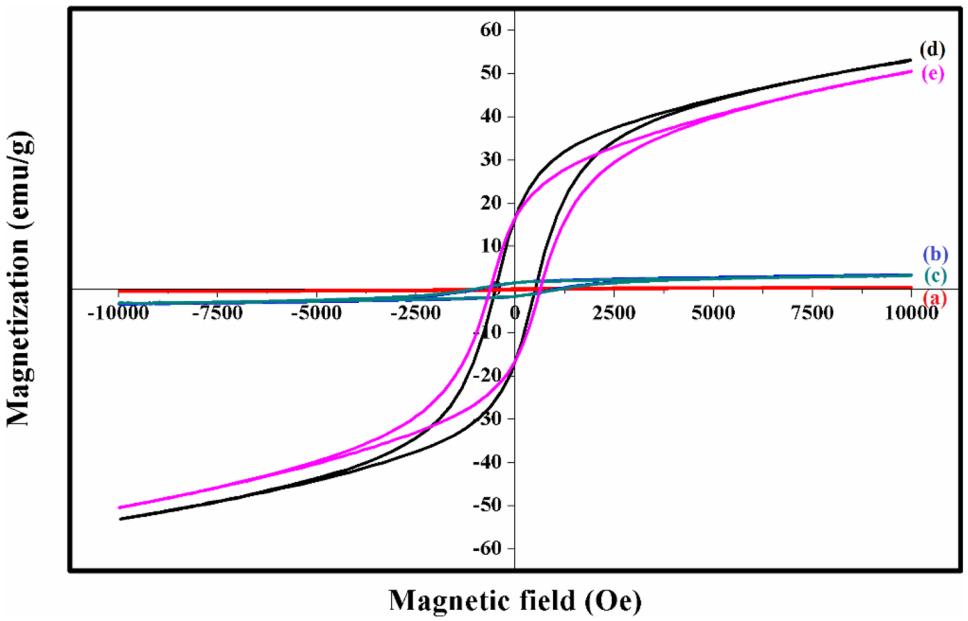


**Fig. 7** VSM hysteresis loops for the obtained powders after calcining the metal complex precursors of the chloride series with Ba:Fe molar ratio of 1:11 at difference temperatures *a* 800, *b* 900, *c* 1000, *d* 1100 and *e* 1200 °C

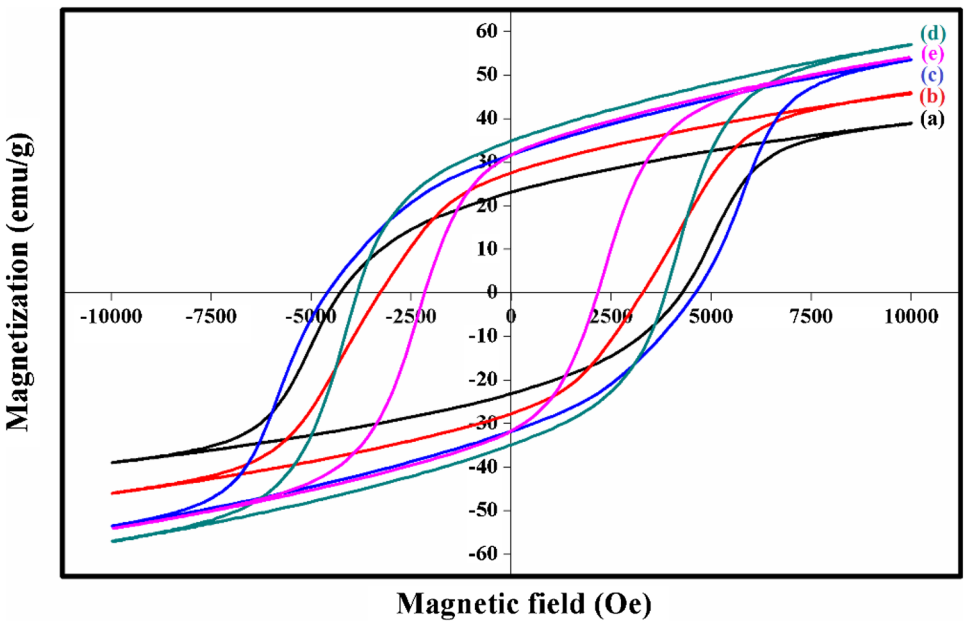


**Fig. 8** VSM hysteresis loops for the obtained powders after calcining the metal complex precursors of the nitrate series with Ba:Fe molar ratio of 1:11 at difference temperatures *a* 800, *b* 900, *c* 1000, *d* 1100 and *e* 1200 °C

SEM images of the prepared powders from the chloride and the nitrate series are shown in Figs. 9 and 10, respectively. SEM images of the powders synthesized from the chloride precursors showed hexagonal shapes related to the hexagonal structure of the barium hexaferrite. The well-defined hexagonal particles are clearly observed for the sample with the calcination temperature of 1100 °C (Fig. 9d). This result was in agreement with the XRD and the VSM results. The impurities found in samples with other calcination temperatures resulted in the imperfect hexagonal particles shape. Unlike the morphologies of the samples from the chloride series, the powders from the nitrate series did not show the hexagonal shape since the nitrate precursors could cause the generation of huge amounts of gases i.e. NO and $NO_2$. The gas formation would obstruct the growth of the hexagonal shape that triggered the irregular shapes with porosity. Therefore, the particles morphologies and sizes was likely to be the factors that affected the coercivity of the prepared materials. As seen from the SEM images, the smaller the particles, the higher the coercivity.

EDX spectra of the powders prepared from the chloride and the nitrate precursors are shown in Figs. 11 and 12.

**Table 3** Average crystalline size (D), average particle size, lattice constants (a, b and c), lattice volume (V), X-ray density ($\rho_x$), saturation magnetization ($M_s$), remanent magnetization ($M_r$) and coercivity ($H_c$) of the obtained powders after calcining the metal complex precursors formed by barium nitrate and iron (III) chloride salts at different temperatures from 800 to 1200 °C

| Parameters | Calcination temperature (°C) | | | | |
|---|---|---|---|---|---|
| | 800 | 900 | 1000 | 1100 | 1200 |
| Average crystalline size (nm), (from FWHM) | 44.0600 | 31.4900 | 35.9000 | 44.0900 | 44.1400 |
| Average particle size (μm), (from SEM) | 3.0200 | 3.9200 | 4.9000 | 5.0600 | 6.6400 |
| a (Å) | * | * | * | 5.7949 | 5.8712 |
| b (Å) | * | * | * | 5.7949 | 5.8712 |
| c (Å) | * | * | * | 22.7461 | 23.1679 |
| V ($Å^3$) | * | * | * | 661.4977 | 691.6257 |
| $\rho_x$ ($g/cm^3$) | * | * | * | 5.5794 | 5.3364 |
| $M_s$ (emu/g) | 0.5157 | 3.3949 | 3.2124 | 50.4576 | 53.0850 |
| $M_r$ (emu/g) | 0.1612 | 1.5298 | 1.5476 | 16.1456 | 16.6540 |
| $M_r/M_s$ | 0.3125 | 0.4506 | 0.4817 | 0.3199 | 0.3137 |
| $H_c$ (kOe) | 1.1801 | 1.0147 | 1.0147 | 0.6853 | 0.5040 |

*The samples have no diffraction peaks of the barium ferrite hexagonal phase to calculate

**Table 4** Average crystalline size (D), average particle size, lattice constants (a, b and c), lattice volume (V), X-ray density ($\rho_x$), saturation magnetization ($M_s$), remanent magnetization ($M_r$) and coercivity ($H_c$) of the obtained powders after calcining the metal complex precursors formed by barium nitrate and iron(III) nitrate salts at different temperatures from 800 to 1200 °C

| Parameters | Calcination temperature (°C) | | | | |
|---|---|---|---|---|---|
| | 800 | 900 | 1000 | 1100 | 1200 |
| Average crystalline size (nm), (from FWHM) | 44.1900 | 44.2000 | 36.8000 | 36.8200 | 44.1200 |
| Average particle size (μm), (from SEM) | 0.1400 | 0.3300 | 0.3900 | 0.5300 | 1.8400 |
| a (Å) | 5.8001 | 5.7871 | 5.8344 | 5.8046 | 5.8952 |
| b (Å) | 5.8001 | 5.7871 | 5.8344 | 5.8046 | 5.8952 |
| c (Å) | 22.8497 | 22.7545 | 22.9310 | 22.8123 | 23.2241 |
| V ($Å^3$) | 665.7054 | 659.9635 | 675.9989 | 665.6475 | 698.974 |
| $\rho_x$ ($g/cm^3$) | 5.5441 | 5.9240 | 5.4597 | 5.5446 | 5.2802 |
| $M_s$ (emu/g) | 39.0165 | 45.8219 | 53.5452 | 56.9942 | 50.1282 |
| $M_r$ (emu/g) | 23.0743 | 27.5169 | 31.6676 | 34.1849 | 29.4242 |
| $M_r/M_s$ | 0.5895 | 0.6005 | 0.5914 | 0.5998 | 0.5870 |
| $H_c$ (kOe) | 4.2666 | 3.3028 | 4.5866 | 3.7852 | 2.4890 |

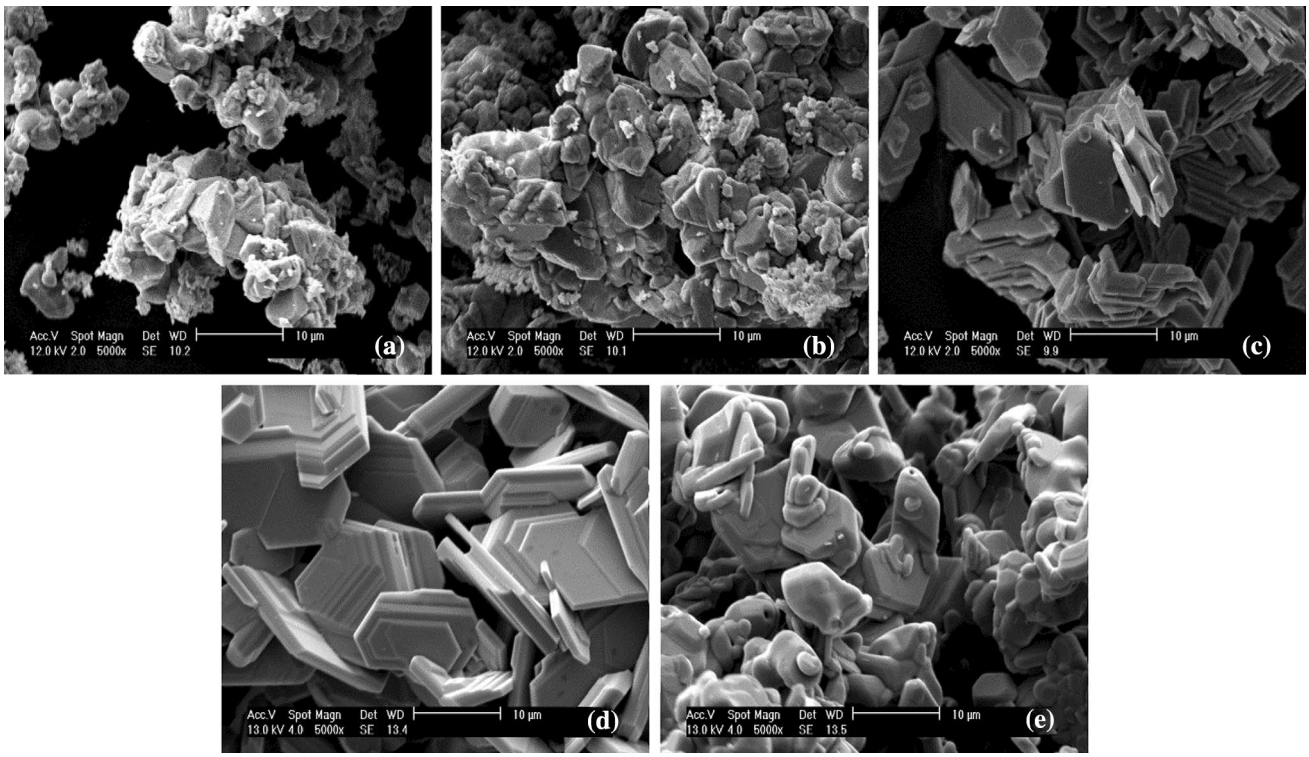


**Fig. 9** SEM images for the obtained powders after calcining the metal complex precursors of the chloride series with Ba:Fe molar ratio of 1:11 at difference temperatures **a** 800, **b** 900, **c** 1000, **d** 1100 and **e** 1200 °C

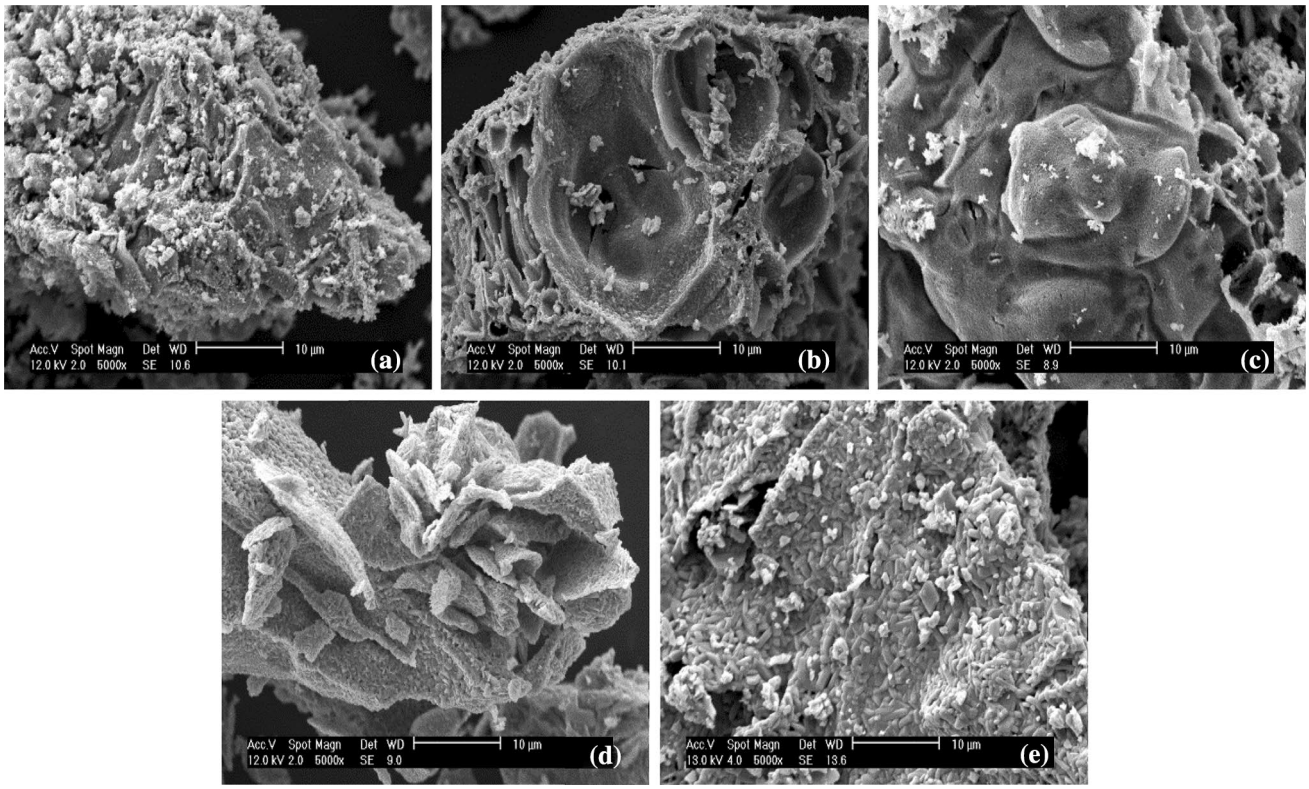


**Fig. 10** SEM images for the obtained powders after calcining the metal complex precursors of the nitrate series with Ba:Fe molar ratio of 1:11 at difference temperatures **a** 800, **b** 900, **c** 1000, **d** 1100 and **e** 1200 °C

The characteristic X-ray fluorescent peak of chloride species was observed in the EDX spectrum of the powder with the Ba:Fe ratio of 1:11 calcined at 1100 °C of the chloride series. This revealed that chloride cannot be eliminated from the sample even when a high temperature is used in the synthesis. It was believed that the chloride is substituted the oxide within the structure of barium hexaferrite since no others impure-crystalline phases were recognized according to the XRD patterns. This substitution may cause the distortion of the structure of the barium hexaferrite, and may be the reason of the significant drop in the coercivity. Herein, we reveal that the material properties synthesized by the thermal decomposition method are varied and can be controlled by the choice of metal-complex precursors, which also observed in the cases of ceria-based materials in our previous works [36–38].

## 4 Conclusions

The barium hexaferrite powders were prepared by the modified Pechini method using citrate and glycerol as the ligand for the formation of metal complex precursors. By varying the synthetic conditions, i.e. Ba:Fe ratios, iron(III) precursor salts and calcination temperatures, the powders with the different magnetic properties were obtained. XRD results showed that the most suitable Ba:Fe molar ratio was 1:11 for both the chloride and the nitrate series indicating by the presence of only the crystalline barium hexaferrite phase. The other ratios resulted in the lower in magnetization saturation due to the presence of the antiferromagnetic barium monoferrite and the non-ferromagnetic α-hematite. The lowest calcination temperature that gave the pure barium hexaferrite phase for the chloride series was 1100 °C. No barium hexaferrite (or only small amounts) was formed in the chloride series at temperature lower than 1100 °C, confirmed by XRD and VSM. For the nitrate series, barium hexaferrite was found as a major phase mixed with barium monoferrite and α-hematite minor phases at 800 °C. The higher temperature allowed the barium monoferrite to react with α-hematite and finally obtain the higher purity of barium hexaferrite product. The most appropriate calcination temperature was also 1100 °C which offered the highest magnetic properties for the materials. The temperature higher than 1200 °C led to the particle agglomeration which resulted in the lower saturation magnetization. Comparing between different series, the powders obtained from the chloride precursors had significantly lower coercive fields than those of the nitrate precursors. The reasons were likely to be the

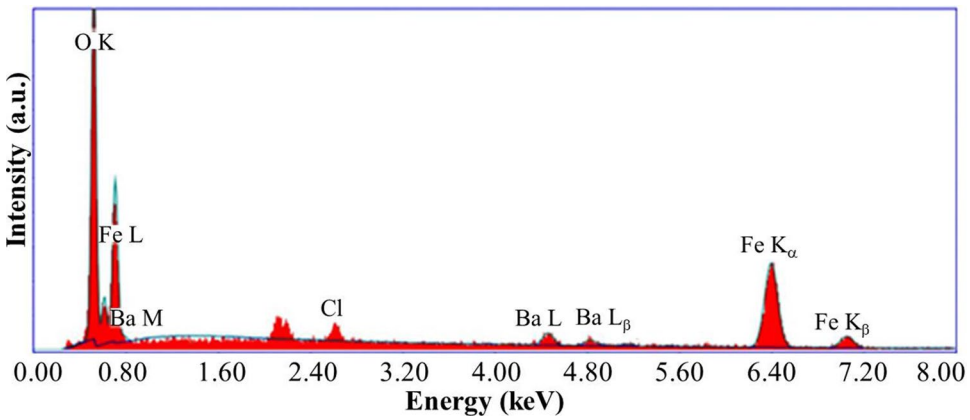


**Fig. 11** EDX spectrum of barium hexaferrite powder obtained from the chloride series by calcined at 1100 °C for 2 h

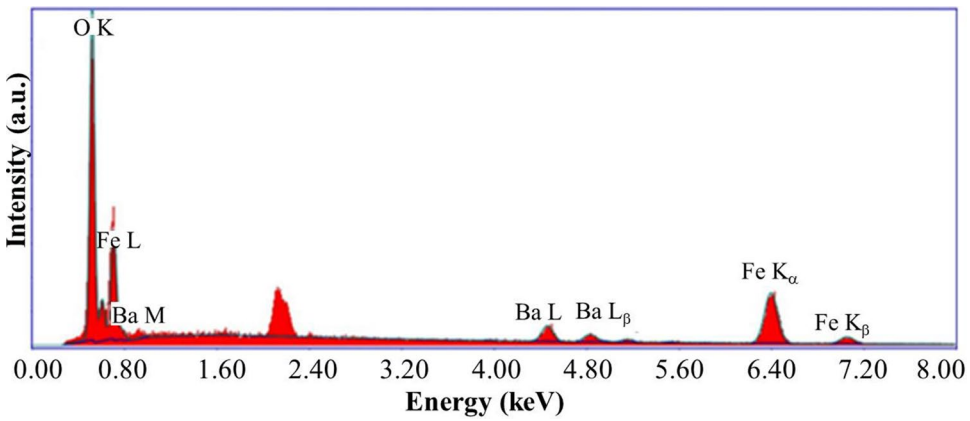


**Fig. 12** EDX spectrum of barium hexaferrite powder obtained from the nitrate series by calcined at 1000 °C for 2 h

smaller particle sizes in materials obtained from the nitrate series. Moreover, the chloride species possibly substituted some of the oxide within the barium hexaferrite structure (indicating by the presence of chloride species in EDX spectra) leading to the distortion of the structure and consequently the significant lower of coercivity.

**Acknowledgements** This work was supported by Kasetsart University Research and Development Institute (KURDI), Department of Chemistry, Faculty of Science, Kasetsart University and Department of Materials Engineering, Faculty of Engineering, Kasetsart University.

## References

1. V.A.M. Brabers, Handb. Magnet. Mater. **8** 189–324 (1995)
2. J.L. Dormann, M. Nogues, J. Phys. Condens. Matter **2**, 1223–1237 (1990)
3. D.S. Mathew, R.-S. Juang, Chem. Eng. J. **129**, 51–65 (2007)
4. R.C. Pullar, Prog. Mater. Sci. **57** 1191–1334 (2012)
5. F. Li, J. Liu, D.G. Evans, X. Duan, Chem. Mater. **16**, 1597–1602 (2004)
6. M. Rahimi-Nasrabadi, M. Behpour, A. Sobhani-Nasab, S.M. Hosseinpour-Mashkani, J. Mater. Sci. **26**, 9776–9781 (2015)
7. A. Javidan, M. Ramezani, A. Sobhani-Nasab, S.M. Hosseinpour-Mashkani, J. Mater. Sci. **26**, 3813–3818 (2015)
8. A. Sobhani-Nasab, Z. Zahraei, M. Akbari, M. Maddahfar, S.M. Hosseinpour-Mashkani, J. Mol. Struct. **1139**, 430–435 (2017)
9. H. Shang, J. Wang, Q. Liu, Mater. Sci. Eng., **456**, 130–132 (2007)
10. U. Topal, H. Ozkan, L. Dorosinskii, J. Alloys Compds. **428**, 17–21 (2007)
11. S. Castro, M. Gayoso, J. Rivas, J.M. Greneche, J. Mira, C. Rodríguez, J. Magnet. Magnet. Mater. **152**, 61–69 (1996)
12. S.S. Fortes, J.G.S. Duque, M.A. Macêdo, Phys. B **384**, 88–90 (2006)
13. R.C. Pullar, A.K. Bhattacharya, Mater. Lett. **57**, 537–542 (2002)
14. P. Xu, X. Han, H. Zhao, Z. Liang, J. Wang, Mater. Lett. **62**, 1305–1308 (2008)
15. W. Zhong, N. Zhang, J. Hong, Q.J. Yan, Y.W. Du, J. Magnet. Magnet. Mater. **168**, 196–202 (1997)
16. K. Haneda, C. Miyakawa, H. Kojima, J. Am. Ceram. Soc. **57**, 354–357 (1974)
17. D. Barb, L. Diamandescu, A. Rusi, D. TĂrĂbĂsanu-MihĂilĂ, M. Morariu, V. Teodorescu, J. Mater. Sci. **21**, 1118–1122 (1986)
18. D. Mishra, S. Anand, R.K. Panda, R.P. Das, Mater. Chem. Phys. **86**, 132–136 (2004)
19. R.B. Jotania, R.B. Khomane, C.C. Chauhan, S.K. Menon, B.D. Kulkarni, J. Magn. Magn. Mater. **320**, 1095–1101 (2008)
20. L. Rezlescu, E. Rezlescu, P.D. Popa, N. Rezlescu, J. Magnet. Magnet. Mater. **193**, 288–290 (1999)
21. S.G. Doh, E.B. Kim, B.H. Lee, J.H. Oh, J. Magnet. Magnet. Mater. **272–276**, 2238–2240 (2004)
22. M.M. Rashad, I.A. Ibrahim, J. Magn. Magn. Mater. **323**, 2158–2164 (2011)
23. P. Kumara, A. Gaura, R.K. Kotnala, Ceram. Int. **43**, 1180–1185 (2017)

24. W. Zhong, W. Chen, W.P. Ding, N. Zhang, A. Hu, Y.W. .Du, Q.J. Yan, J. Magnet. Magnet. Mater. **195**, 112–118 (1999)
25. A. Ataie, A. Mali, J. Electroceram. **21**, 357–360 (2008)
26. E.D. Solovyova, M.L. Calzada, A.G. Belous, J. Sol Gel Sci. Technol. **75**, 215–223 (2015)
27. E. Matijevic, J. Colloid Interface Sci. **117** 593–595 (1987)
28. V. Pillai, P. Kumar, D.O. Shah, J. Magnet. Magnet. Mater. **116**, 299–304 (1992)
29. Z.X. Tang, S. Nafis, C.M. Sorensen, G.C. Hadjipanayis, K.J. Klabunde, IEEE Tran. Magnet. **25**, 4236–4238 (1989)
30. Y.Y. Meng, M.H. He, Q. Zeng, D.L. Jiao, S. Shukla, R.V. Ramanujan, Z.W. Liu, J. Alloys Compds. **583**, 220–225 (2014)
31. O. Carp, R. Barjega, E. Segal, M. Brezeanu, Thermochim. Acta **318**, 57–62 (1998)
32. G. Mendoza-Suarez, M.C. Cisneros-Morales, M.M. Cisneros-Guerrero, K.K. Johal, H. Mancha-Molinar, O.E. Ayala-Valenzuela, J.I. Escalante-Garcia, Mater. Chem. Phys. **77**, 796–801 (2002)
33. F. Yen-Pei, L. Cheng-Hsiung, P. Ko-Ying, Japn. J. Appl. Phys. **42**, 2681–2684 (2003)
34. J. Huang, H. Zhuang, W. Li, Mater. Res. Bull. **38**, 149–159 (2003)
35. G. Mendoza-Suarez, J.A. Matutes-Aquino, J.I. Escalante-Garcia, H. Mancha-Molinar, D. Rios-Jara, K.K. Johal, J. Magnet. Magnet. Mater. **223**, 55–62 (2001)
36. W. Wattanathana, N. Nootsuwan, C. Veranitisagul, N. Koonsaeng, N. Laosiripojana, A. Laobuthee, J. Mol. Struct. **1089**, 9–15 (2015)
37. W. Wattanathana, C. Veranitisagul, S. Wannapaiboon, W. Klysubun, N. Koonsaeng, A. Laobuthee, Ceram. Int. **43**, 9823–9830 (2017)
38. W. Wattanathana, S. Wannapaiboon, C. Veranitisagul, N. Laosiripojana, N. Koonsaeng, A. Laobuthee, Adv. Mater. Sci. Eng. (2017). doi:10.1155/2017/5828067